

Observation of $D \rightarrow a_0(980)\pi$ in the decays $D^0 \rightarrow \pi^+\pi^-\eta$ and $D^+ \rightarrow \pi^+\pi^0\eta$

M. Ablikim¹, M. N. Achasov^{4,c}, P. Adlarson⁷⁵, O. Afedulidis³, X. C. Ai⁸⁰, R. Aliberti³⁵, A. Amoroso^{74A,74C}, Q. An^{71,58,a}, Y. Bai⁵⁷, O. Bakina³⁶, I. Balossino^{29A}, Y. Ban^{46,h}, H.-R. Bao⁶³, V. Batzskaya^{1,44}, K. Begzsuren³², N. Berger³⁵, M. Berlowski⁴⁴, M. Bertani^{28A}, D. Bettoni^{29A}, F. Bianchi^{74A,74C}, E. Bianco^{74A,74C}, A. Bortone^{74A,74C}, I. Boyko³⁶, R. A. Briere⁵, A. Brueggemann⁶⁸, H. Cai⁷⁶, X. Cai^{1,58}, A. Calcaterra^{28A}, G. F. Cao^{1,63}, N. Cao^{1,63}, S. A. Cetin^{62A}, J. F. Chang^{1,58}, G. R. Che⁴³, G. Chelkov^{36,b}, C. Chen⁴³, C. H. Chen⁹, Chao Chen⁵⁵, G. Chen¹, H. S. Chen^{1,63}, H. Y. Chen²⁰, M. L. Chen^{1,58,63}, S. J. Chen⁴², S. L. Chen⁴⁵, S. M. Chen⁶¹, T. Chen^{1,63}, X. R. Chen^{31,63}, X. T. Chen^{1,63}, Y. B. Chen^{1,58}, Y. Q. Chen³⁴, Z. J. Chen^{25,i}, Z. Y. Chen^{1,63}, S. K. Choi^{10A}, G. Cibinetto^{29A}, F. Cossio^{74C}, J. J. Cui⁵⁰, H. L. Dai^{1,58}, J. P. Dai⁷⁸, A. Dbeyssi¹⁸, R. E. de Boer³, D. Dedovich³⁶, C. Q. Deng⁷², Z. Y. Deng¹, A. Denig³⁵, I. Denysenko³⁶, M. Destefanis^{74A,74C}, F. De Mori^{74A,74C}, B. Ding^{66,1}, X. X. Ding^{46,h}, Y. Ding³⁴, Y. Ding⁴⁰, J. Dong^{1,58}, L. Y. Dong^{1,63}, M. Y. Dong^{1,58,63}, X. Dong⁷⁶, M. C. Du¹, S. X. Du⁸⁰, Y. Y. Duan⁵⁵, Z. H. Duan⁴², P. Egorov^{36,b}, Y. H. Fan⁴⁵, J. Fang⁵⁹, J. Fang^{1,58}, S. S. Fang^{1,63}, W. X. Fang¹, Y. Fang¹, Y. Q. Fang^{1,58}, R. Farinelli^{29A}, L. Fava^{74B,74C}, F. Feldbauer³, G. Felici^{28A}, C. Q. Feng^{1,58}, J. H. Feng⁵⁹, Y. T. Feng^{71,58}, M. Fritsch³, C. D. Fu¹, J. L. Fu⁶³, Y. W. Fu^{1,63}, H. Gao⁶³, X. B. Gao⁴¹, Y. N. Gao^{46,h}, Yang Gao^{71,58}, S. Garbolino^{74C}, I. Garzia^{29A,29B}, L. Ge⁸⁰, P. T. Ge⁷⁶, Z. W. Ge⁴², C. Geng⁵⁹, E. M. Gersabeck⁶⁷, A. Gilman⁶⁹, K. Goetzen¹³, L. Gong⁴⁰, W. X. Gong^{1,58}, W. Gradl³⁵, S. Gramigna^{29A,29B}, M. Greco^{74A,74C}, M. H. Gu^{1,58}, Y. T. Gu¹⁵, C. Y. Guan^{1,63}, A. Q. Guo^{31,63}, L. B. Guo⁴¹, M. J. Guo⁵⁰, R. P. Guo⁴⁹, Y. P. Guo^{12,g}, A. Guskov^{36,b}, J. Gutierrez²⁷, K. L. Han⁶³, T. T. Han¹, F. Hanisch³, X. Q. Hao¹⁹, F. A. Harris⁶⁵, K. K. He⁵⁵, K. L. He^{1,63}, F. H. Heinsius³, C. H. Heinz³⁵, Y. K. Heng^{1,58,63}, C. Herold⁶⁰, T. Holtmann³, P. C. Hong³⁴, G. Y. Hou^{1,63}, X. T. Hou^{1,63}, Y. R. Hou⁶³, Z. L. Hou¹, B. Y. Hu⁵⁹, H. M. Hu^{1,63}, J. F. Hu^{56,j}, S. L. Hu^{12,g}, T. Hu^{1,58,63}, Y. Hu¹, G. S. Huang^{71,58}, K. X. Huang⁵⁹, L. Q. Huang^{31,63}, X. T. Huang⁵⁰, Y. P. Huang¹, Y. S. Huang⁵⁹, T. Hussain⁷³, F. Hölzken³, N. Hüskens³⁵, N. in der Wiesche⁶⁸, J. Jackson²⁷, S. Janchiv³², J. H. Jeong^{10A}, Q. Ji¹, Q. P. Ji¹⁹, W. Ji^{1,63}, X. B. Ji^{1,63}, X. L. Ji^{1,58}, Y. Y. Ji⁵⁰, X. Q. Jia⁵⁰, Z. K. Jia^{71,58}, D. Jiang^{1,63}, H. B. Jiang⁷⁶, P. C. Jiang^{46,h}, S. S. Jiang³⁹, T. J. Jiang¹⁶, X. S. Jiang^{1,58,63}, Y. Jiang⁶³, J. B. Jiao⁵⁰, J. K. Jiao³⁴, Z. Jiao²³, S. Jin⁴², Y. Jin⁶⁶, M. Q. Jing^{1,63}, X. M. Jing⁶³, T. Johansson⁷⁵, S. Kabana³³, N. Kalantar-Nayestanaki⁶⁴, X. L. Kang⁹, X. S. Kang⁴⁰, M. Kavatsyuk⁶⁴, B. C. Ke⁸⁰, V. Khachatryan²⁷, A. Khoukaz⁶⁸, R. Kiuchi¹, O. B. Kolcu^{62A}, B. Kopf³, M. Kuessner³, X. Kui^{1,63}, N. Kumar²⁶, A. Kupsc^{44,75}, W. Kühn³⁷, J. J. Lane⁶⁷, L. Lavezzi^{74A,74C}, T. T. Lei^{71,58}, Z. H. Lei^{71,58}, M. Lellmann³⁵, T. Lenz³⁵, C. Li⁴⁷, C. Li⁴³, C. H. Li³⁹, Cheng Li^{71,58}, D. M. Li⁸⁰, F. Li^{1,58}, G. Li¹, H. B. Li^{1,63}, H. J. Li¹⁹, H. N. Li^{56,j}, Hui Li⁴³, J. R. Li⁶¹, J. S. Li⁵⁹, K. Li¹, L. J. Li^{1,63}, L. K. Li¹, Lei Li⁴⁸, M. H. Li⁴³, P. R. Li^{38,k,l}, Q. M. Li^{1,63}, Q. X. Li⁵⁰, R. Li^{17,31}, S. X. Li¹², T. Li⁵⁰, W. D. Li^{1,63}, W. G. Li^{1,a}, X. Li^{1,63}, X. H. Li^{71,58}, X. L. Li⁵⁰, X. Y. Li^{1,63}, X. Z. Li⁵⁹, Y. G. Li^{46,h}, Z. J. Li⁵⁹, Z. Y. Li⁷⁸, C. Liang⁴², H. Liang^{1,63}, D. X. Lin^{31,63}, Y. F. Liang⁵⁴, Y. T. Liang^{31,63}, G. R. Liao¹⁴, Y. P. Liao^{1,63}, J. Libby²⁶, A. Limphirat⁶⁰, C. C. Lin⁵⁵, D. X. Lin^{31,63}, T. Lin¹, B. J. Liu¹, B. X. Liu⁷⁶, C. Liu³⁴, C. X. Liu¹, F. Liu¹, F. H. Liu⁵³, Feng Liu⁶, G. M. Liu^{56,j}, H. Liu^{38,k,l}, H. B. Liu¹⁵, H. H. Liu¹, H. M. Liu^{1,63}, Huihui Liu²¹, J. B. Liu^{71,58}, J. Y. Liu^{1,63}, K. Liu^{38,k,l}, K. Y. Liu⁴⁰, Ke Liu²², L. Liu^{71,58}, L. C. Liu⁴³, Lu Liu⁴³, M. H. Liu^{12,g}, P. L. Liu¹, Q. Liu⁶³, S. B. Liu^{71,58}, T. Liu^{12,g}, W. K. Liu⁴³, W. M. Liu^{71,58}, X. Liu^{38,k,l}, X. Liu³⁹, Y. Liu⁸⁰, Y. Liu^{38,k,l}, Y. B. Liu⁴³, Z. A. Liu^{1,58,63}, Z. D. Liu⁹, Z. Q. Liu⁵⁰, X. C. Lou^{1,58,63}, F. X. Lu⁵⁹, H. J. Lu²³, J. G. Lu^{1,58}, X. L. Lu¹, Y. Lu⁷, Y. P. Lu^{1,58}, Z. H. Lu^{1,63}, C. L. Luo⁴¹, J. R. Luo⁵⁹, M. X. Luo⁷⁹, T. Luo^{12,g}, X. L. Luo^{1,58}, X. R. Lyu⁶³, Y. F. Lyu⁴³, F. C. Ma⁴⁰, H. Ma⁷⁸, H. L. Ma¹, J. L. Ma^{1,63}, L. L. Ma⁵⁰, M. M. Ma^{1,63}, Q. M. Ma¹, R. Q. Ma^{1,63}, T. Ma^{71,58}, X. T. Ma^{1,63}, X. Y. Ma^{1,58}, Y. Ma^{46,h}, Y. M. Ma³¹, F. E. Maas¹⁸, M. Maggiora^{74A,74C}, S. Malde⁶⁹, Y. J. Mao^{46,h}, Z. P. Mao¹, S. Marcello^{74A,74C}, Z. X. Meng⁶⁶, J. G. Messchendorp^{13,64}, G. Mezzadri^{29A}, H. Miao^{1,63}, T. J. Min⁴², R. E. Mitchell²⁷, X. H. Mo^{1,58,63}, B. Moses²⁷, N. Yu. Muchnoi^{4,c}, J. Muskalla³⁵, Y. Nefedov³⁶, F. Nerling^{18,e}, L. S. Nie²⁰, I. B. Nikolaev^{4,c}, Z. Ning^{1,58}, S. Nisar^{11,m}, Q. L. Niu^{38,k,l}, W. D. Niu⁵⁵, Y. Niu⁵⁰, S. L. Olsen⁶³, Q. Ouyang^{1,58,63}, S. Pacetti^{28B,28C}, X. Pan⁵⁵, Y. Pan⁵⁷, A. Pathak³⁴, Y. P. Pei^{71,58}, M. Pelizaeus³, H. P. Peng^{71,58}, Y. Y. Peng^{38,k,l}, K. Peters^{13,e}, J. L. Ping⁴¹, R. G. Ping^{1,63}, S. Plura³⁵, V. Prasad³³, F. Z. Qi¹, H. Qi^{71,58}, H. R. Qi⁶¹, M. Qi⁴², T. Y. Qi^{12,g}, S. Qian^{1,58}, W. B. Qian⁶³, C. F. Qiao⁶³, X. K. Qiao⁸⁰, J. J. Qin⁷², L. Q. Qin¹⁴, L. Y. Qin^{71,58}, X. P. Qin^{12,g}, X. S. Qin⁵⁰, Z. H. Qin^{1,58}, J. F. Qiu¹, Z. H. Qu⁷², C. F. Redmer³⁵, K. J. Ren³⁹, A. Rivetti^{74C}, M. Rolo^{74C}, G. Rong^{1,63}, Ch. Rosner¹⁸, S. N. Ruan⁴³, N. Salone⁴⁴, A. Sarantsev^{36,d}, Y. Schelhaas³⁵, K. Schoenning⁷⁵, M. Scodreggio^{29A}, K. Y. Shan^{12,g}, W. Shan²⁴, X. Y. Shan^{71,58}, Z. J. Shang^{38,k,l}, J. F. Shangguan¹⁶, L. G. Shao^{1,63}, M. Shao^{71,58}, C. P. Shen^{12,g}, H. F. Shen¹⁸, W. H. Shen⁶³, X. Y. Shen^{1,63}, B. A. Shi⁶³, H. Shi^{71,58}, H. C. Shi^{71,58}, J. L. Shi^{12,g}, J. Y. Shi¹, Q. Q. Shi⁵⁵, S. Y. Shi⁷², X. Shi^{1,58}, J. J. Song¹⁹, T. Z. Song⁵⁹, W. M. Song^{34,1}, Y. J. Song^{12,g}, Y. X. Song^{46,h,n}, S. Sosio^{74A,74C}, S. Spataro^{74A,74C}, F. Stielers³⁵, Y. J. Su⁶³, G. B. Sun⁷⁶, G. X. Sun¹, H. Sun⁶³, H. K. Sun¹, J. F. Sun¹⁹, K. Sun⁶¹, L. Sun⁷⁶, S. S. Sun^{1,63}, T. Sun^{51,f}, W. Y. Sun³⁴, Y. Sun⁹, Y. J. Sun^{71,58}, Y. Z. Sun¹, Z. Q. Sun^{1,63}, Z. T. Sun⁵⁰, C. J. Tang⁵⁴, G. Y. Tang¹, J. Tang⁵⁹, M. Tang^{71,58}, Y. A. Tang⁷⁶, L. Y. Tao⁷², Q. T. Tao^{25,i}, M. Tat⁶⁹, J. X. Teng^{71,58}, V. Thoren⁷⁵, W. H. Tian⁵⁹, Y. Tian^{31,63}, Z. F. Tian⁷⁶, I. Uman^{62B}, Y. Wan⁵⁵, S. J. Wang⁵⁰, B. Wang¹, B. L. Wang⁶³, Bo Wang^{71,58}, D. Y. Wang^{46,h}, F. Wang⁷², H. J. Wang^{38,k,l}, J. J. Wang⁷⁶, J. P. Wang⁵⁰, K. Wang^{1,58}, L. L. Wang¹, M. Wang⁵⁰, N. Y. Wang⁶³, S. Wang^{12,g}, S. Wang^{38,k,l}, T. Wang^{12,g}, T. J. Wang⁴³, W. Wang⁵⁹, W. Wang⁷², W. P. Wang^{35,71,o}, X. Wang^{46,h}, X. F. Wang^{38,k,l}, X. J. Wang³⁹, X. L. Wang^{12,g}, X. N. Wang¹, Y. Wang⁶¹, Y. D. Wang⁴⁵, Y. F. Wang^{1,58,63}, Y. L. Wang¹⁹, Y. N. Wang⁴⁵, Y. Q. Wang¹, Yaqian Wang¹⁷, Yi Wang⁶¹, Z. Wang^{1,58}, Z. L. Wang⁷², Z. Y. Wang^{1,63}, Ziyi Wang⁶³, D. H. Wei¹⁴, F. Weidner⁶⁸, S. P. Wen¹, Y. R. Wen³⁹, U. Wiedner³, G. Wilkinson⁶⁹, M. Wolke⁷⁵, L. Wollenberg³, C. Wu³⁹, J. F. Wu^{1,8}, L. H. Wu¹, L. J. Wu^{1,63}, X. Wu^{12,g}, X. H. Wu³⁴, Y. Wu^{71,58}, Y. H. Wu⁵⁵, Y. J. Wu³¹, Z. Wu^{1,58}, L. Xia^{71,58}, X. M. Xian³⁹, B. H. Xiang^{1,63}, T. Xiang^{46,h}, D. Xiao^{38,k,l}, G. Y. Xiao⁴², S. Y. Xiao¹, Y. L. Xiao^{12,g}, Z. J. Xiao⁴¹, C. Xie⁴², X. H. Xie^{46,h}, Y. Xie⁵⁰, Y. G. Xie^{1,58}, Y. H. Xie⁶, Z. P. Xie^{71,58}, T. Y. Xing^{1,63}, C. F. Xu^{1,63}, C. J. Xu⁵⁹, G. F. Xu¹, H. Y. Xu^{66,2,p}, M. Xu^{71,58}, Q. J. Xu¹⁶, Q. N. Xu³⁰, W. Xu¹, W. L. Xu⁶⁶, X. P. Xu⁵⁵, Y. C. Xu⁷⁷, Z. S. Xu⁶³, F. Yan^{12,g}, L. Yan^{12,g}, W. B. Yan^{71,58}, W. C. Yan⁸⁰, X. Q. Yan¹,

H. J. Yang^{51,f}, H. L. Yang³⁴, H. X. Yang¹, T. Yang¹, Y. Yang^{12,g}, Y. F. Yang^{1,63}, Y. F. Yang⁴³, Y. X. Yang^{1,63},
 Z. W. Yang^{38,k,l}, Z. P. Yao⁵⁰, M. Ye^{1,58}, M. H. Ye⁸, J. H. Yin¹, Z. Y. You⁵⁹, B. X. Yu^{1,58,63}, C. X. Yu⁴³, G. Yu^{1,63},
 J. S. Yu^{25,i}, T. Yu⁷², X. D. Yu^{46,h}, Y. C. Yu⁸⁰, C. Z. Yuan^{1,63}, J. Yuan³⁴, J. Yuan⁴⁵, L. Yuan², S. C. Yuan^{1,63}, Y. Yuan^{1,63},
 Z. Y. Yuan⁵⁹, C. X. Yue³⁹, A. A. Zafar⁷³, F. R. Zeng⁵⁰, S. H. Zeng⁷², X. Zeng^{12,g}, Y. Zeng^{25,i}, Y. J. Zeng⁵⁹, Y. J. Zeng^{1,63},
 X. Y. Zhai³⁴, Y. C. Zhai⁵⁰, Y. H. Zhan⁵⁹, A. Q. Zhang^{1,63}, B. L. Zhang^{1,63}, B. X. Zhang¹, D. H. Zhang⁴³, G. Y. Zhang¹⁹,
 H. Zhang⁸⁰, H. Zhang^{71,58}, H. C. Zhang^{1,58,63}, H. H. Zhang³⁴, H. H. Zhang⁵⁹, H. Q. Zhang^{1,58,63}, H. R. Zhang^{71,58},
 H. Y. Zhang^{1,58}, J. Zhang⁸⁰, J. Zhang⁵⁹, J. J. Zhang⁵², J. L. Zhang²⁰, J. Q. Zhang⁴¹, J. S. Zhang^{12,g}, J. W. Zhang^{1,58,63},
 J. X. Zhang^{38,k,l}, J. Y. Zhang¹, J. Z. Zhang^{1,63}, Jianyu Zhang⁶³, L. M. Zhang⁶¹, Lei Zhang⁴², P. Zhang^{1,63}, Q. Y. Zhang³⁴,
 R. Y. Zhang^{38,k,l}, S. H. Zhang^{1,63}, Shulei Zhang^{25,i}, X. D. Zhang⁴⁵, X. M. Zhang¹, X. Y. Zhang⁵⁰, Y. Zhang⁷², Y. Zhang¹,
 Y. T. Zhang⁸⁰, Y. H. Zhang^{1,58}, Y. M. Zhang³⁹, Yan Zhang^{71,58}, Z. D. Zhang¹, Z. H. Zhang¹, Z. L. Zhang³⁴, Z. Y. Zhang⁷⁶,
 Z. Y. Zhang⁴³, Z. Z. Zhang⁴⁵, G. Zhao¹, J. Y. Zhao^{1,63}, J. Z. Zhao^{1,58}, L. Zhao¹, Lei Zhao^{71,58}, M. G. Zhao⁴³, N. Zhao⁷⁸,
 R. P. Zhao⁶³, S. J. Zhao⁸⁰, Y. B. Zhao^{1,58}, Y. X. Zhao^{31,63}, Z. G. Zhao^{71,58}, A. Zhemchugov^{36,b}, B. Zheng⁷², B. M. Zheng³⁴,
 J. P. Zheng^{1,58}, W. J. Zheng^{1,63}, Y. H. Zheng⁶³, B. Zhong⁴¹, X. Zhong⁵⁹, H. Zhou⁵⁰, J. Y. Zhou³⁴, L. P. Zhou^{1,63}, S. Zhou⁶,
 X. Zhou⁷⁶, X. K. Zhou⁶, X. R. Zhou^{71,58}, X. Y. Zhou³⁹, Y. Z. Zhou^{12,g}, J. Zhu⁴³, K. Zhu¹, K. J. Zhu^{1,58,63}, K. S. Zhu^{12,g},
 L. Zhu³⁴, L. X. Zhu⁶³, S. H. Zhu⁷⁰, T. J. Zhu^{12,g}, W. D. Zhu⁴¹, Y. C. Zhu^{71,58}, Z. A. Zhu^{1,63}, J. H. Zou¹, J. Zu^{71,58}

(BESIII Collaboration)

¹ Institute of High Energy Physics, Beijing 100049, People's Republic of China

² Beihang University, Beijing 100191, People's Republic of China

³ Bochum Ruhr-University, D-44780 Bochum, Germany

⁴ Budker Institute of Nuclear Physics SB RAS (BINP), Novosibirsk 630090, Russia

⁵ Carnegie Mellon University, Pittsburgh, Pennsylvania 15213, USA

⁶ Central China Normal University, Wuhan 430079, People's Republic of China

⁷ Central South University, Changsha 410083, People's Republic of China

⁸ China Center of Advanced Science and Technology, Beijing 100190, People's Republic of China

⁹ China University of Geosciences, Wuhan 430074, People's Republic of China

¹⁰ Chung-Ang University, Seoul, 06974, Republic of Korea

¹¹ COMSATS University Islamabad, Lahore Campus, Defence Road, Off Raiwind Road, 54000 Lahore, Pakistan

¹² Fudan University, Shanghai 200433, People's Republic of China

¹³ GSI Helmholtzcentre for Heavy Ion Research GmbH, D-64291 Darmstadt, Germany

¹⁴ Guangxi Normal University, Guilin 541004, People's Republic of China

¹⁵ Guangxi University, Nanning 530004, People's Republic of China

¹⁶ Hangzhou Normal University, Hangzhou 310036, People's Republic of China

¹⁷ Hebei University, Baoding 071002, People's Republic of China

¹⁸ Helmholtz Institute Mainz, Staudinger Weg 18, D-55099 Mainz, Germany

¹⁹ Henan Normal University, Xinxiang 453007, People's Republic of China

²⁰ Henan University, Kaifeng 475004, People's Republic of China

²¹ Henan University of Science and Technology, Luoyang 471003, People's Republic of China

²² Henan University of Technology, Zhengzhou 450001, People's Republic of China

²³ Huangshan College, Huangshan 245000, People's Republic of China

²⁴ Hunan Normal University, Changsha 410081, People's Republic of China

²⁵ Hunan University, Changsha 410082, People's Republic of China

²⁶ Indian Institute of Technology Madras, Chennai 600036, India

²⁷ Indiana University, Bloomington, Indiana 47405, USA

²⁸ INFN Laboratori Nazionali di Frascati, (A)INFN Laboratori Nazionali di Frascati, I-00044, Frascati, Italy; (B)INFN

Sezione di Perugia, I-06100, Perugia, Italy; (C)University of Perugia, I-06100, Perugia, Italy

²⁹ INFN Sezione di Ferrara, (A)INFN Sezione di Ferrara, I-44122, Ferrara, Italy; (B)University of Ferrara, I-44122, Ferrara, Italy

³⁰ Inner Mongolia University, Hohhot 010021, People's Republic of China

³¹ Institute of Modern Physics, Lanzhou 730000, People's Republic of China

³² Institute of Physics and Technology, Peace Avenue 54B, Ulaanbaatar 13330, Mongolia

³³ Instituto de Alta Investigación, Universidad de Tarapacá, Casilla 7D, Arica 1000000, Chile

³⁴ Jilin University, Changchun 130012, People's Republic of China

³⁵ Johannes Gutenberg University of Mainz, Johann-Joachim-Becher-Weg 45, D-55099 Mainz, Germany

³⁶ Joint Institute for Nuclear Research, 141980 Dubna, Moscow region, Russia

³⁷ Justus-Liebig-Universität Giessen, II. Physikalisches Institut, Heinrich-Buff-Ring 16, D-35392 Giessen, Germany

³⁸ Lanzhou University, Lanzhou 730000, People's Republic of China

³⁹ Liaoning Normal University, Dalian 116029, People's Republic of China

⁴⁰ Liaoning University, Shenyang 110036, People's Republic of China

⁴¹ Nanjing Normal University, Nanjing 210023, People's Republic of China

⁴² Nanjing University, Nanjing 210093, People's Republic of China

⁴³ Nankai University, Tianjin 300071, People's Republic of China

⁴⁴ National Centre for Nuclear Research, Warsaw 02-093, Poland

- ⁴⁵ North China Electric Power University, Beijing 102206, People's Republic of China
- ⁴⁶ Peking University, Beijing 100871, People's Republic of China
- ⁴⁷ Qufu Normal University, Qufu 273165, People's Republic of China
- ⁴⁸ Renmin University of China, Beijing 100872, People's Republic of China
- ⁴⁹ Shandong Normal University, Jinan 250014, People's Republic of China
- ⁵⁰ Shandong University, Jinan 250100, People's Republic of China
- ⁵¹ Shanghai Jiao Tong University, Shanghai 200240, People's Republic of China
- ⁵² Shanxi Normal University, Linfen 041004, People's Republic of China
- ⁵³ Shanxi University, Taiyuan 030006, People's Republic of China
- ⁵⁴ Sichuan University, Chengdu 610064, People's Republic of China
- ⁵⁵ Soochow University, Suzhou 215006, People's Republic of China
- ⁵⁶ South China Normal University, Guangzhou 510006, People's Republic of China
- ⁵⁷ Southeast University, Nanjing 211100, People's Republic of China
- ⁵⁸ State Key Laboratory of Particle Detection and Electronics, Beijing 100049, Hefei 230026, People's Republic of China
- ⁵⁹ Sun Yat-Sen University, Guangzhou 510275, People's Republic of China
- ⁶⁰ Suranaree University of Technology, University Avenue 111, Nakhon Ratchasima 30000, Thailand
- ⁶¹ Tsinghua University, Beijing 100084, People's Republic of China
- ⁶² Turkish Accelerator Center Particle Factory Group, (A)Istinye University, 34010, Istanbul, Turkey; (B)Near East University, Nicosia, North Cyprus, 99138, Mersin 10, Turkey
- ⁶³ University of Chinese Academy of Sciences, Beijing 100049, People's Republic of China
- ⁶⁴ University of Groningen, NL-9747 AA Groningen, The Netherlands
- ⁶⁵ University of Hawaii, Honolulu, Hawaii 96822, USA
- ⁶⁶ University of Jinan, Jinan 250022, People's Republic of China
- ⁶⁷ University of Manchester, Oxford Road, Manchester, M13 9PL, United Kingdom
- ⁶⁸ University of Muenster, Wilhelm-Klemm-Strasse 9, 48149 Muenster, Germany
- ⁶⁹ University of Oxford, Keble Road, Oxford OX13RH, United Kingdom
- ⁷⁰ University of Science and Technology Liaoning, Anshan 114051, People's Republic of China
- ⁷¹ University of Science and Technology of China, Hefei 230026, People's Republic of China
- ⁷² University of South China, Hengyang 421001, People's Republic of China
- ⁷³ University of the Punjab, Lahore-54590, Pakistan
- ⁷⁴ University of Turin and INFN, (A)University of Turin, I-10125, Turin, Italy; (B)University of Eastern Piedmont, I-15121, Alessandria, Italy; (C)INFN, I-10125, Turin, Italy
- ⁷⁵ Uppsala University, Box 516, SE-75120 Uppsala, Sweden
- ⁷⁶ Wuhan University, Wuhan 430072, People's Republic of China
- ⁷⁷ Yantai University, Yantai 264005, People's Republic of China
- ⁷⁸ Yunnan University, Kunming 650500, People's Republic of China
- ⁷⁹ Zhejiang University, Hangzhou 310027, People's Republic of China
- ⁸⁰ Zhengzhou University, Zhengzhou 450001, People's Republic of China
- ^a Deceased
- ^b Also at the Moscow Institute of Physics and Technology, Moscow 141700, Russia
- ^c Also at the Novosibirsk State University, Novosibirsk, 630090, Russia
- ^d Also at the NRC "Kurchatov Institute", PNPI, 188300, Gatchina, Russia
- ^e Also at Goethe University Frankfurt, 60323 Frankfurt am Main, Germany
- ^f Also at Key Laboratory for Particle Physics, Astrophysics and Cosmology, Ministry of Education; Shanghai Key Laboratory for Particle Physics and Cosmology; Institute of Nuclear and Particle Physics, Shanghai 200240, People's Republic of China
- ^g Also at Key Laboratory of Nuclear Physics and Ion-beam Application (MOE) and Institute of Modern Physics, Fudan University, Shanghai 200443, People's Republic of China
- ^h Also at State Key Laboratory of Nuclear Physics and Technology, Peking University, Beijing 100871, People's Republic of China
- ⁱ Also at School of Physics and Electronics, Hunan University, Changsha 410082, China
- ^j Also at Guangdong Provincial Key Laboratory of Nuclear Science, Institute of Quantum Matter, South China Normal University, Guangzhou 510006, China
- ^k Also at MOE Frontiers Science Center for Rare Isotopes, Lanzhou University, Lanzhou 730000, People's Republic of China
- ^l Also at Lanzhou Center for Theoretical Physics, Lanzhou University, Lanzhou 730000, People's Republic of China
- ^m Also at the Department of Mathematical Sciences, IBA, Karachi 75270, Pakistan
- ⁿ Also at Ecole Polytechnique Federale de Lausanne (EPFL), CH-1015 Lausanne, Switzerland
- ^o Also at Helmholtz Institute Mainz, Staudinger Weg 18, D-55099 Mainz, Germany
- ^p Also at School of Physics, Beihang University, Beijing 100191, China

We report the first amplitude analysis of the decays $D^0 \rightarrow \pi^+\pi^-\eta$ and $D^+ \rightarrow \pi^+\pi^0\eta$ using

a data sample taken with the BESIII detector at the center-of-mass energy of 3.773 GeV, corresponding to an integrated luminosity of 7.9 fb^{-1} . The contribution from the process $D^{0(+)} \rightarrow a_0(980)^+ \pi^{-(0)}$ is significantly larger than the $D^{0(+)} \rightarrow a_0(980)^-(0) \pi^+$ contribution. The ratios $\mathcal{B}(D^0 \rightarrow a_0(980)^+ \pi^-) / \mathcal{B}(D^0 \rightarrow a_0(980)^- \pi^+)$ and $\mathcal{B}(D^+ \rightarrow a_0(980)^+ \pi^0) / \mathcal{B}(D^+ \rightarrow a_0(980)^0 \pi^+)$ are measured to be $7.5_{-0.8}^{+2.5}_{\text{stat.}} \pm 1.7_{\text{syst.}}$ and $2.6 \pm 0.6_{\text{stat.}} \pm 0.3_{\text{syst.}}$, respectively. The measured D^0 ratio disagrees with the theoretical predictions by orders of magnitudes, thus implying a substantial contribution from final-state interactions.

Theoretical predictions of the strong interaction in the charm sector are challenging, since quantum chromodynamics calculations involve non-perturbative contributions. The W-annihilation (WA) and W-exchange (WE) processes, which are strictly suppressed in B -meson decays, can occur in D decays as a result of final-state interactions (FSI). They are expected to be dominated by non-perturbative effects, which leads to significant uncertainties when making theoretical predictions, since these effects depend strongly on the cutoff values and the unknown phases between different processes [1, 2]. Therefore, the study of decays with a significant contribution from WA or WE processes represents a promising method for investigating the dynamics of charm decays.

The BESIII Collaboration has observed the pure WA decays $D_s^+ \rightarrow a_0(980)^+(0) \pi^{0(+)}$ [3], which indicates a sizeable contribution from FSI in the WA processes for the $D \rightarrow SP$ sector (where S and P denote scalar and pseudo-scalar particles, respectively). Theorists have explained the observed large WA amplitude, as well as the amplitude symmetry $A(D_s^+ \rightarrow a_0(980)^+ \pi^0) = -A(D_s^+ \rightarrow a_0(980)^0 \pi^+)$, taking into account the contribution from the $D_s^+ \rightarrow \rho^+ \eta$ and $D_s^+ \rightarrow \bar{K}^*(892)^0 K^+(K^*(892)^+ \bar{K}^0)$ decays, since they exhibit large branching fractions (BF) and involve the WA amplitude process at the quark level [4, 5]. This behavior supports the interpretations of $a_0(980)$ as a tetraquark or a molecular state [5]. More recently, further measurements involving D_s^+ decays have been performed, in particular those that have led to the observation of the $a_0(1817)^+(0)$ resonance [6, 7], which is expected as an excited state of the $a_0(980)^+(0)$ [8], support the interpretation of these two resonances as $K^{(*)} \bar{K}^{(*)}$ molecules [9, 10].

In D^0 decays, the relative ratio $r_{+/-} = \mathcal{B}(D^0 \rightarrow a_0(980)^+ \pi^-) / \mathcal{B}(D^0 \rightarrow a_0(980)^- \pi^+)$ is expected to be less than 0.05 [11], when ignoring the WE process. Until now, attempts to measure this ratio have not been conclusive; both the CLEO and LHCb Collaborations have studied the $a_0(980)^\pm \pi^\mp$ contributions to the decays $D^0 \rightarrow K_S^0 K^\pm \pi^\mp$ [12, 13], but with large uncertainties; the Belle Collaboration has studied $D^0 \rightarrow \pi^+ \pi^- \eta$ decays [14], and has only observed the $a_0(980)$ peak in the $M(\pi^+ \eta)$ projection.

In analogy to what is observed in $D_s^+ \rightarrow a_0(980)^+(0) \pi^{0(+)}$ decays [3], sizeable contributions from FSI are expected to enhance the WA process in the corresponding D^+ decays. However, in this case the symmetry

observed in D_s^+ decays is expected to be violated, since further short-distance contributions must be considered, which can be expressed as a color-allowed external W -emission tree (T) diagram and a color-suppressed external W -emission tree diagram in the topological diagram approach [11]. The measurement of the BFs for D^0 (D^+) decays to $a_0(980)\pi$ and of the corresponding relative ratios $r_{+/-}$ ($r_{+/0} = \mathcal{B}(D^+ \rightarrow a_0(980)^+ \pi^0) / \mathcal{B}(D^+ \rightarrow a_0(980)^0 \pi^+)$) can constrain the size and phase of the amplitude of the WE (WA) process and improve the knowledge about the role the $a_0(980)$ plays in charm decays [15].

In this Letter, we perform amplitude analyses of $D^{0(+)} \rightarrow \pi^+ \pi^{-(0)} \eta$ decays, to study the contributions from the intermediate processes $D^{0(+)} \rightarrow a_0(980)^+ \pi^{-(0)}$, $D^{0(+)} \rightarrow a_0(980)^-(0) \pi^+$ and $D^{0(+)} \rightarrow \rho^{0(+)} \eta$. The analyses are based on e^+e^- collision data recorded with the BESIII detector at the center-of-mass energy of 3.773 GeV, corresponding to an integrated luminosity of 7.9 fb^{-1} . Charge conjugation is implied throughout this Letter, as well as the equivalences $a_0(980)^\pm(0) \rightarrow \pi^\pm(0) \eta$ and $\mathcal{B}(a_0(980)^+ \rightarrow \pi^+ \eta) = \mathcal{B}(a_0(980)^0 \rightarrow \pi^0 \eta)$.

A detailed description of the BESIII detector design and performance can be found in Ref. [16]. About 63% of the data analyzed in this Letter profits from an upgrade of the end-cap time-of-flight system with multi-gap resistive plate chambers with a time resolution of 60 ps [17]. Simulated data samples produced with a GEANT4-based [19] Monte Carlo (MC) package, which includes the geometric description of the BESIII detector and the detector response, are used to determine detection efficiencies and to estimate backgrounds. The simulation models the beam-energy spread and initial-state radiation (ISR) in e^+e^- annihilations with the generator KKMC [20]. The inclusive MC sample includes the production of $D\bar{D}$ pairs (including quantum coherence for the neutral D channels), the non- $D\bar{D}$ decays of the $\psi(3770)$, the ISR production of the J/ψ and $\psi(3686)$ states, and the continuum processes incorporated in KKMC [20].

The charged-track selection, particle identification (PID), K_S^0 , π^0 and η reconstruction use the same criteria described in Ref. [3], except for the invariant-mass window around the η , which is set to $0.45 < M(\gamma\gamma)_\eta < 0.55 \text{ GeV}/c^2$. The D mesons are identified using the beam-constrained mass $M_{\text{BC}} = \sqrt{E_{\text{beam}}^2 - |\vec{P}_D|^2}$ and the deviation of the reconstructed energy from the expected

energy $\Delta E = E_D - E_{\text{beam}}$, where (E_D, \vec{P}_D) is the four-momentum of the D meson, and E_{beam} is the beam energy. A double-tag (DT) technique [21] is employed to suppress the background. On both the tag and the signal side, any candidate with $M_{\text{BC}} < 1.83 \text{ GeV}/c^2$ or $|\Delta E| > 0.1 \text{ GeV}$ is rejected; if multiple combinations survive in an event, the one with the M_{BC} closest to the known D meson mass from Particle Data Group (PDG) [18] is retained.

For the D^0 channel, four tag modes ($\bar{D}^0 \rightarrow K^+\pi^-$, $\bar{D}^0 \rightarrow K^+\pi^-\pi^0(\pi^0)$ and $\bar{D}^0 \rightarrow K^+\pi^-\pi^-\pi^+$) are used, while for the D^+ channel we use six tag modes ($D^- \rightarrow K^+\pi^-\pi^-(\pi^0)$, $D^- \rightarrow K_S^0\pi^-(\pi^0)$, $D^- \rightarrow K_S^0\pi^-\pi^-\pi^+$ and $D^- \rightarrow K^+K^-\pi^-$). Signal MC samples with $\psi(3770) \rightarrow D\bar{D}$, $\bar{D} \rightarrow \text{tag modes}$ and $D \rightarrow \text{signal modes}$ are produced, in which the signal decays $D^{0(+)} \rightarrow \pi^+\pi^{-(0)}\eta$ are generated with the amplitude models that result from the studies presented in this Letter. For the tag channels, the M_{BC} signal windows are set to be $\pm 6 \text{ MeV}/c^2$ around the known D mass [18], while the ΔE signal windows are set to be 3.5 times the ΔE resolution around the fitted peak.

On the signal side, we select D^0 (D^+) candidates with M_{BC} within $[1.858, 1.874] \text{ GeV}/c^2$ ($[1.860, 1.880] \text{ GeV}/c^2$). Furthermore, for the D^0 channel, the requirement $|M(\pi^+\pi^-) - m(K_S^0)| > 0.03 \text{ GeV}/c^2$ is imposed to remove the peaking background from the $D^0 \rightarrow K_S^0\eta$ decays, where $m(K_S^0)$ is the known K_S^0 mass [18]. Since the dominant background originates from wrong $\eta \rightarrow \gamma\gamma$ candidates, a multivariate analysis (MVA) [22] is performed to select events for use in the amplitude analysis. This MVA involves the development of a Gradient Boosted Decision Tree (BDTG) classifier based on the inclusive MC sample, which operates on three discriminating variables: the $\gamma\gamma$ invariant mass $M(\gamma\gamma)_\eta$, the goodness of the kinematic fit constraining the $\gamma\gamma$ invariant mass to the known η mass $\chi^2(\eta)$, and the helicity angle of the higher energy photon from the η decay. A requirement on the BDTG output is imposed, which retains 83% (77%) of the signal and rejects 78% (84%) of the background for the D^0 (D^+) channel according to studies performed with MC simulation. Additionally, the selection $|\Delta E| < 0.045 \text{ GeV}$ ($|\Delta E| < 0.040 \text{ GeV}$) for the D^0 (D^+) channel is applied. The final sample contains 1678 (1226) D^0 (D^+) $\rightarrow \pi^+\pi^-(\pi^0)\eta$ candidates with a purity of $(74.1 \pm 1.2)\%$ ($(65.7 \pm 1.7)\%$).

The amplitude analysis is performed on the accepted candidate events with an unbinned maximum-likelihood fit. The logarithm of the likelihood is constructed as

$$\ln L = \ln(f_s \tilde{S}(p) + (1 - f_s) \tilde{B}(p)), \quad (1)$$

where f_s is the signal purity, p is the four-momenta of final particles, $\tilde{S}(p)$ and $\tilde{B}(p)$ are the signal and back-

ground probability density function (PDF), expressed as

$$\begin{aligned} \tilde{S}(p) &= \frac{\epsilon(p)|\mathcal{M}(p)|^2 R_3(p)}{\int \epsilon(p)|\mathcal{M}(p)|^2 R_3(p) dp}, \\ \tilde{B}(p) &= \frac{\epsilon(p)B_\epsilon(p)R_3(p)}{\int \epsilon(p)B_\epsilon(p)R_3(p) dp}. \end{aligned} \quad (2)$$

Here, $R_3(p)$ is the three-body phase-space factor, $\epsilon(p)$ is the efficiency function, $\mathcal{M}(p)$ is the signal amplitude, $B(p)$ is the background shape, and $B_\epsilon(p) = B(p)/\epsilon(p)$ is the efficiency-corrected background shape. For the D^0 channel, the $B(p)$ term is extracted from the ΔE sideband region ($0.05 < |\Delta E| < 0.10 \text{ GeV}$); for the D^+ channel, since the resolution is much wider than for the D^0 , the inclusive MC sample is used. The total signal amplitude $\mathcal{M}(p) = \sum_\alpha c_\alpha e^{i\phi_\alpha} A_\alpha$ is modeled as the coherent sum of the amplitudes of all the intermediate processes, where c_α and ϕ_α are the magnitude and phase of the α^{th} amplitude, respectively, and the α^{th} amplitude is given by $A_\alpha = P_\alpha S_\alpha F_\alpha^r F_\alpha^D$. Here, P_α is the propagator, generally following the relativistic Breit-Wigner formula except for the ρ and $a_0(980)$ states. For the ρ^+ we use the GS formula [23], and for the ρ^0 description $\rho - \omega$ mixing is additionally considered [24]. When modeling the $a_0(980)$ the two channel-coupled Flatté formula $P_{a_0(980)} = 1/[(m_0^2 - s_a) - i(g_{\eta\pi}^2 \rho_{\eta\pi} + g_{K\bar{K}}^2 \rho_{K\bar{K}})]$ is used, with $g_{\pi\eta}$ ($g_{K\bar{K}}$) and $\rho_{\pi\eta}$ ($\rho_{K\bar{K}}$) representing the coupling constant from Ref. [25] and the phase-space factor $q/\sqrt{s_a}$, respectively, where s_a is the invariant-mass squared of the $a_0(980)$ candidate and q is the total momentum of the daughter particles in the $a_0(980)$ rest frame. For $\pi^+\pi^-$ S -wave scattering, the K-matrix formalism [26] is used, with parameters taken from Ref. [27]. The S_α term is the spin factor and is constructed with the covariant-tensor formalism [28]. The F_α^r (F_α^D) term is the barrier factor for the intermediate state (the D meson) [7]. The relative contribution of the α^{th} amplitude to the β^{th} amplitude is quantified by the ratio $r_{\alpha/\beta} = \int |c_\alpha A_\alpha(p)|^2 R_3(p) dp / \int |c_\beta A_\beta(p)|^2 R_3(p) dp$. When substituting $c_\beta A_\beta$ with $\mathcal{M}(p)$, the ratio becomes the fit fraction of the α^{th} amplitude (FF $_\alpha$).

In the data projections, a significant ρ^0 peak appears for the D^0 channel, while for the D^+ channel there is no evident ρ^+ peak but a significant $a_0(980)^+$ peak is observed. Therefore, the decays $D^0 \rightarrow \rho^0\eta$ and $D^+ \rightarrow a_0(980)^+\pi^0$ are chosen as the reference amplitudes for the D^0 and D^+ channels, respectively. All contributions with significance larger than 3σ are retained for further analysis. Here, the significance is calculated using the changes of $\ln L$ and the number of degrees of freedom (NDF) when the fit is performed with and without the corresponding amplitude included. Following this criterion, six intermediate states are retained in the fit model for both channels. The decay amplitudes and the corresponding ϕ_α , FF $_\alpha$, significance, BF, and $r_{+/- (0)}$ values are listed in Table I. The Dalitz plots and the projec-

TABLE I. The phases, FFs, statistical significances and BFs for various amplitudes. The first and second uncertainties are statistical and systematic, respectively. The intermediate states are reconstructed in the decays $\rho \rightarrow \pi\pi$, $a_0 \rightarrow \pi\eta$ and $a_2 \rightarrow \pi\eta$.

Amplitude	Phase (in unit rad)	FF (%)	Significance (σ)	BF ($\times 10^{-3}$)
$D^0 \rightarrow \rho^0\eta$	0 (fixed)	$15.2 \pm 1.7 \pm 1.0$	> 10	$0.19 \pm 0.02 \pm 0.01$
$D^0 \rightarrow a_0(980)^-\pi^+$	$0.06 \pm 0.16 \pm 0.12$	$5.9 \pm 1.3 \pm 1.0$	8.9	$0.07 \pm 0.02 \pm 0.01$
$D^0 \rightarrow a_0(980)^+\pi^-$	$-1.06 \pm 0.12 \pm 0.10$	$44.0 \pm 4.0 \pm 5.3$	> 10	$0.55 \pm 0.05 \pm 0.07$
$D^0 \rightarrow a_2(1320)^+\pi^-$	$-1.16 \pm 0.25 \pm 0.23$	$2.1 \pm 0.9 \pm 0.8$	4.5	$0.03 \pm 0.01 \pm 0.01$
$D^0 \rightarrow a_2(1700)^+\pi^-$	$0.08 \pm 0.17 \pm 0.23$	$5.5 \pm 1.8 \pm 2.7$	6.1	$0.07 \pm 0.02 \pm 0.03$
$D^0 \rightarrow (\pi^+\pi^-)_{S\text{-wave}}\eta$	$-0.92 \pm 0.29 \pm 0.14$	$3.9 \pm 1.8 \pm 2.1$	5.3	$0.05 \pm 0.02 \pm 0.03$
$r_{+/-}$		$7.5^{+2.5}_{-0.8} \pm 1.7$	7.7*	-
$D^+ \rightarrow \rho^+\eta$	$-4.03 \pm 0.19 \pm 0.13$	$9.3 \pm 3.0 \pm 2.1$	6.0	$0.20 \pm 0.07 \pm 0.05$
$D^+ \rightarrow (\pi^+\pi^0)_{V}\eta$	$-0.64 \pm 0.22 \pm 0.19$	$15.8 \pm 4.8 \pm 5.2$	4.7	$0.34 \pm 0.11 \pm 0.11$
$D^+ \rightarrow a_0(980)^+\pi^0$	0 (fixed)	$43.7 \pm 5.6 \pm 1.9$	9.1	$0.95 \pm 0.12 \pm 0.05$
$D^+ \rightarrow a_0(980)^0\pi^+$	$2.44 \pm 0.20 \pm 0.10$	$17.0 \pm 4.4 \pm 1.7$	7.9	$0.37 \pm 0.10 \pm 0.04$
$D^+ \rightarrow a_2(1700)^+\pi^0$	$0.92 \pm 0.20 \pm 0.14$	$4.2 \pm 2.1 \pm 0.7$	3.6	$0.09 \pm 0.05 \pm 0.02$
$D^+ \rightarrow a_0(1450)^+\pi^0$	$0.63 \pm 0.41 \pm 0.30$	$7.0 \pm 2.8 \pm 0.7$	4.7	$0.15 \pm 0.06 \pm 0.02$
$r_{+/0}$		$2.6 \pm 0.6 \pm 0.3$	4.0*	-

* The significance is for the test hypothesis $r = 1.0$.

tions are shown in Fig. 1. The fit quality is determined by calculating the χ^2 of the fit using an adaptive binning of the $M^2(\pi^+\eta)$ versus $M^2(\pi^-\eta)$ ($M^2(\pi^0\eta)$) Dalitz plot with each bin containing at least 10 events. The resulting χ^2/NDF is 136.6/138 (131.6/99) for the $D^0(D^+)$ channel.

In Table I, the second uncertainties are systematic and arise from the following sources: (I) the coupling with the $\pi\eta'$ channel in the $a_0(980)$ line shape [25]; (II) the $a_0(980)^\pm$ mass and coupling constants, changed within the uncertainties given by Ref. [25]; (III) the masses and widths of the ρ^0 , $a_2(1320)^+$ and $a_2(1700)^+$ states, changed within the uncertainties given by PDG [18]; (IV) the parameters in the K-matrix formalism, changed within the statistical uncertainties given in Ref. [27] (only for the D^0 channel); (V) the effective radii for the intermediate resonances and for the $D^{0(+)}$ state, estimated by varying the effective radii by ± 1 GeV $^{-1}$; (VI) the background level, estimated from the uncertainty of the signal ratio in data; (VII) the background shape, estimated by checking the effect on the fit results with background shapes extracted from the different sideband regions; (VIII) the fitter performance, estimated by fitting three hundred signal MC samples with the same size as the data sample. The fits show good agreement between the fitted and the input values for the parameters in the amplitude model. These systematic uncertainties are estimated separately by taking the difference between the values of ϕ_α , FF_α , $r_{+/-}$ and $r_{+/0}$ obtained by the alternative and the baseline fits. Since varying the propagators causes different normalization factors, only the effect on the FF_α is considered [3] from source (I) for the corresponding amplitudes, which is also similar for source (IV). The total systematic uncertainties are obtained by adding each term in quadrature.

The BFs of each sub-process in Table I are calculated

with $\mathcal{B}_\alpha = \text{FF}_\alpha \times \mathcal{B}(D^{0(+)} \rightarrow \pi^+\pi^{-(0)}\eta)$. In the BF measurements, tighter windows than those used for the MVA selections, $0.505 < M(\gamma\gamma)_\eta < 0.570$ GeV/ c^2 and $\chi^2(\eta) < 50$, are used. The total decay BFs are measured with the DT method as $\mathcal{B} = Y_{\text{DT}}/Y_{\text{ST}}\epsilon_{\text{sig}}\mathcal{B}_{\text{sub}}$; here, Y_{ST} is the total single tag (ST) yield, which is $(6897.1 \pm 8.2) \times 10^3$ [$(4176.9 \pm 2.8) \times 10^3$] for the D^0 (D^+) channel; \mathcal{B}_{sub} is the BF of $\pi^0(\eta) \rightarrow \gamma\gamma$; ϵ_{sig} is the weighted signal efficiency $\epsilon_{\text{sig}} = \sum_i \frac{Y_{\text{ST}}^{(i)}}{\epsilon_{\text{ST}}^{(i)}} \epsilon_{\text{DT}}^{(i)}/Y_{\text{ST}}$, where the $Y_{\text{ST}}^{(i)}$ and $\epsilon_{\text{ST}}^{(i)}$ are the ST yield and ST (DT) efficiencies for the i^{th} tag channels, respectively. The DT yields Y_{DT} are extracted using a fit to the ΔE distributions without applying the signal window, as shown in Fig. 2. In the fit, the signal PDF is parameterized as the sum of a bifurcated Gaussian [30] and a double Gaussian function, where the two functions have the same mean value. All the parameters except for the mean value are determined by the fit to the signal MC sample. The background function is described by a second-order Chebyshev polynomial, validated by using the inclusive MC sample. From the fits, we obtain $Y_{\text{DT}}(D^0) = 1369 \pm 48$ and $Y_{\text{DT}}(D^+) = 949 \pm 54$.

The total BFs of the $D^0 \rightarrow \pi^+\pi^-\eta$ and $D^+ \rightarrow \pi^+\pi^0\eta$ channels are measured to be $(1.24 \pm 0.04_{\text{stat.}} \pm 0.03_{\text{syst.}}) \times 10^{-3}$ and $(2.18 \pm 0.12_{\text{stat.}} \pm 0.05_{\text{syst.}}) \times 10^{-3}$, respectively. Here, the systematic uncertainties for the D^0 and D^+ channels include: PID (1.0% and 0.5%); tracking efficiency (1.0% and 0.5%); η/π^0 reconstruction (0.8% and 1.6%), determined from hadronic DT $D\bar{D}$ events; signal shape (0.3% and 0.1%), estimated by the change of Y_{DT} by altering the parameters in the signal shape within the uncertainties; background shape (0.6% and 1.4%), estimated by using a third-order Chebyshev polynomial instead of the second-order one; M_{BC} window (0.3% and 0.0%), determined with the $D^0 \rightarrow K^-\pi^+\eta$ control sam-

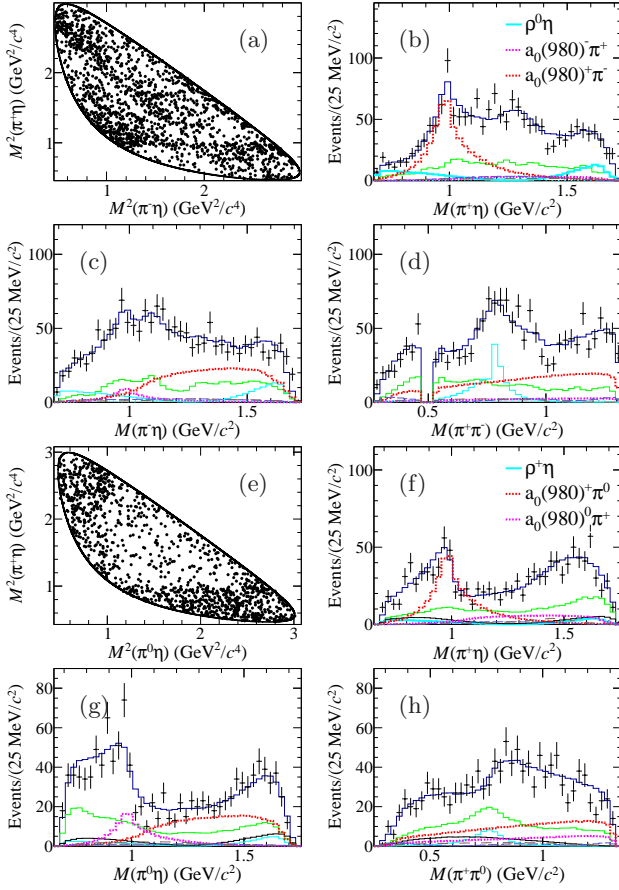


FIG. 1. The Dalitz plot (a), the projections on $M(\pi^+\eta)$ (b), $M(\pi^-\eta)$ (c), $M(\pi^+\pi^-)$ (d) for the $D^0 \rightarrow \pi^+\pi^-\eta$ channel and the Dalitz plot (e), the projections on $M(\pi^+\eta)$ (f), $M(\pi^0\eta)$ (g), $M(\pi^+\pi^0)$ (h) for the $D^+ \rightarrow \pi^+\pi^0\eta$ channel. In the projections, the dots with error bars are data, the blue lines are the fit curves and the green histograms are the backgrounds; the cyan solid, pink dashed and red dashed lines are the contributions from the intermediate states $\rho^{0(+)}$, $a_0(980)^{-(0)}$ and $a_0(980)^+$, respectively.

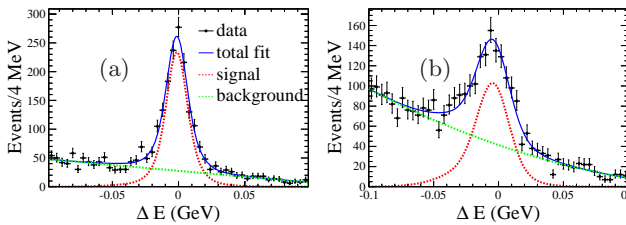


FIG. 2. Fits to the ΔE distributions for (a) $D^0 \rightarrow \pi^+\pi^-\eta$ and (b) $D^+ \rightarrow \pi^+\pi^0\eta$. The dots with error bars are data. The blue solid, red dashed and green dashed lines are the total fit, the signal and the background contribution, respectively.

ple for the D^0 channel and negligible for the D^+ channel due to the loose window requirement; MC sample size (0.1% and 0.1%); quantum correlations (0.9%, only for the D^0 channel), quoted from Ref. [31]; fitter performance (0.3% and 0.6%), estimated from the inclusive MC sample; MC generator (0.2% and 0.4%), estimated by varying the input parameters in the generator according to the error matrix obtained from the fit to data; uncertainties from $\mathcal{B}(\eta/\pi^0 \rightarrow \gamma\gamma)$ (0.5% and 0.5%), quoted from the PDG [18].

From the amplitude model we calculate the ratios $r_{+/-} = 7.5_{-0.8}^{+2.5}_{\text{stat.}} \pm 1.7_{\text{syst.}}$ and $r_{+/0} = 2.6 \pm 0.6_{\text{stat.}} \pm 0.3_{\text{syst.}}$, which are both significantly higher than unity. Especially for the D^0 channel, the $r_{+/-}$ higher than the results of naive calculations that do not allow for enhancements to the WE contributions by two orders of magnitude [11].

In summary, we present the first amplitude analysis of the $D^{0(+)} \rightarrow \pi^+\pi^{-(0)}\eta$ channel. The decays $D^{0(+)} \rightarrow a_0(980)^+\pi^{-(0)}$ and $D^{0(+)} \rightarrow a_0(980)^{-(0)}\pi^+$ are observed for the first time with statistical significances $> 10\sigma$ (9.1σ) and 8.9σ (7.9σ), respectively. The $a_0(980)^+$ is identified as the dominant intermediate resonance in both channels, and its contribution is found to be significantly larger than that of the $a_0(980)^{-(0)}$ state.

For the D^+ channel, the measured value of $r_{+/0}$ indicates that the symmetry observed in D_s^+ decays is here violated. Furthermore, in contrast with the large BF of $D_s^+ \rightarrow \rho^+\eta$, the low BF of $D^+ \rightarrow \rho^+\eta$ shows the importance of the $K^*K \rightarrow a_0(980)\pi$ re-scattering process. For the D^0 channel, the measured value of $r_{+/-}$ disagrees with theoretical predictions that ignore non-perturbative effects by two orders of magnitude. Estimations suggest that the size for the amplitude of WE process is even larger than that of the T diagram [11, 32]. This dominance of the WE process in $D \rightarrow SP$ decays is to be contrasted with the situation in $D \rightarrow SP$, $D \rightarrow PP$ and $D \rightarrow VP$ (V denotes vector particle) decays [11, 33], indicating the very important role that FSI plays in the $D \rightarrow SP$ sector. In analogy to theoretical interpretations for WA process, the re-scattering contributions also suggest that we would expect $r_{+/-} < 1$ [34], in contradiction to our measurement. In addition, the resonance $a_0(1817)$ is not observed in both channels. The measured BFs and ratios are highly valuable for improving the understanding of the role that the $a_0(980)$ plays in charm-meson decays and the theoretical interpretations of the nature of the $a_0(980)$ state.

The authors greatly thank Professor H.Y. Cheng from Institute of Physics, Academia Sinica for the useful discussions. The BESIII Collaboration thanks the staff of BEPCII and the IHEP computing center for their strong support. This work is supported in part by National Key R&D Program of China under Contracts Nos.

2023YFA1606000, 2020YFA0406300, 2020YFA0406400; National Natural Science Foundation of China (NSFC) under Contracts Nos. 11635010, 11735014, 11935015, 11935016, 11935018, 11961141012, 12025502, 12035009, 12035013, 12061131003, 12192260, 12192261, 12192262, 12192263, 12192264, 12192265, 12221005, 12225509, 12235017, 12205384, 12361141819; the Chinese Academy of Sciences (CAS) Large-Scale Scientific Facility Program; the CAS Center for Excellence in Particle Physics (CCEPP); Joint Large-Scale Scientific Facility Funds of the NSFC and CAS under Contract No. U1832207, U2032104; 100 Talents Program of CAS; The Institute of Nuclear and Particle Physics (INPAC) and Shanghai Key Laboratory for Particle Physics and Cosmology; German Research Foundation DFG under Contracts Nos. 455635585, FOR5327, GRK 2149; Istituto Nazionale di Fisica Nucleare, Italy; Ministry of Development of Turkey under Contract No. DPT2006K-120470; National Research Foundation of Korea under Contract No. NRF-2022R1A2C1092335; National Science and Technology fund of Mongolia; National Science Research and Innovation Fund (NSRF) via the Program Management Unit for Human Resources & Institutional Development, Research and Innovation of Thailand under Contract No. B16F640076; Polish National Science Centre under Contract No. 2019/35/O/ST2/02907; The Swedish Research Council; U. S. Department of Energy under Contract No. DE-FG02-05ER41374

[1] H. Y. Cheng and C. W. Chiang, Phys. Rev. D **81**, 074021 (2010).
[2] Q. Qin, H. n. Li, C. D. Lü and F. S. Yu, Phys. Rev. D **89**, 054006 (2014).
[3] M. Ablikim *et al.* [BESIII Collaboration], Phys. Rev. Lett. **123**, 112001 (2019).
[4] Y. K. Hsiao, Y. Yu and B. C. Ke, Eur. Phys. J. C **80**, 895 (2020).
[5] X. Z. Ling, M. Z. Liu, J. X. Lu, L. S. Geng and J. J. Xie, Phys. Rev. D **103**, 116016 (2021).
[6] M. Ablikim *et al.* [BESIII Collaboration], Phys. Rev. D **105**, L051103 (2022).
[7] M. Ablikim *et al.* [BESIII Collaboration], Phys. Rev. Lett. **129**, 182001 (2022).
[8] D. Guo, W. Chen, H. X. Chen, X. Liu and S. L. Zhu, Phys. Rev. D **105**, 114014 (2022).
[9] Z. L. Wang and B. S. Zou, Phys. Rev. D **104**, 114001 (2021).
[10] E. Oset, L. R. Dai and L. S. Geng, Sci. Bull. **68**, 243-246 (2023).
[11] H. Y. Cheng, C. W. Chiang and Z. Q. Zhang, Phys. Rev. D **105**, 033006 (2022).
[12] J. Insler *et al.* [CLEO Collaboration], Phys. Rev. D **85**, 092016 (2012) [erratum: Phys. Rev. D **94**, 099905 (2016)].
[13] R. Aaij *et al.* [LHCb Collaboration], Phys. Rev. D **93**, 052018 (2016).

[14] L. K. Li *et al.* [Belle Collaboration], JHEP **09**, 075 (2021).
[15] N. Ikeno, M. Bayar and E. Oset, Eur. Phys. J. C **81**, 377 (2021).
[16] M. Ablikim *et al.* [BESIII Collaboration], Nucl. Instrum. Methods Phys. Res., Sect. A **614**, 345 (2010).
[17] X. Li *et al.*, Radiat. Detect. Technol. Methods **1**, 13 (2017); Y. X. Guo *et al.*, Radiat. Detect. Technol. Methods **1**, 15 (2017); P. Cao *et al.*, Nucl. Instrum. Meth. A **953**, 163053 (2020).
[18] R. L. Workman *et al.* [Particle Data Group], PTEP **2022**, 083C01 (2022).
[19] S. Agostinelli *et al.* [GEANT4 Collaboration], Nucl. Instrum. Meth. A **506**, 250-303 (2003).
[20] S. Jadach, B. F. L. Ward and Z. Was, Phys. Rev. D **63**, 113009 (2001); Comput. Phys. Commun. **130**, 260 (2000).
[21] R. M. Baltrusaitis *et al.* [MARK-III Collaboration], Phys. Rev. Lett. **56**, 2140 (1986).
[22] A. Hocker *et al.*, *TMVA - Toolkit for Multivariate Data Analysis*, PoS **ACAT**, (2007) 040, arXiv: physics/0703039.
[23] G. J. Gounaris, J. J. Sakurai, Phys. Rev. Lett. **21**, 244 (1968).
[24] M. Ablikim *et al.* [BESIII Collaboration], Phys. Rev. D **100**, 072008 (2019).
[25] M. Ablikim *et al.* [BESIII Collaboration], Phys. Rev. D **95**, 032002 (2017).
[26] V. V. Anisovich and A. V. Sarantsev, Eur. Phys. J. A **16**, 229-258 (2003).
[27] R. Aaij *et al.* [LHCb Collaboration], Phys. Rev. D **92**, 032002 (2015).
[28] B. S. Zou and D. V. Bugg, Eur. Phys. J. A **16**, 537-547 (2003).
[29] M. Ablikim *et al.* [BESIII Collaboration], Phys. Rev. D **95**, 072010 (2017).
[30] The bifurcated Gaussian function is the altered Gaussian function with allowing the left width and right width being different.
[31] M. Ablikim *et al.* [BESIII Collaboration], Phys. Rev. D **101**, 052009 (2020).
[32] The diagram for $D^0 \rightarrow a_0(980)^\pm \pi^\mp$ consists of a T diagram and a WE diagram. To estimate the relative size of the WE amplitude over the T amplitude, we set the amplitude of the T diagram in $D^0 \rightarrow a_0(980)^- \pi^+$ to be $1.0e^{i0.0}$, and denote that for the T diagram in $D^0 \rightarrow a_0(980)^+ \pi^-$ to be $be^{i\phi_b}$, those amplitudes for the WE diagrams for $a_0(980)^-$ and $a_0(980)^+$ involved sub-modes to be $xe^{i\phi_-}$ and $cx e^{i\phi_+}$, respectively, and write $r_{+/-}$ as r for brevity. Here, the parameters b , c and x are real numbers. According to how the relative BF is determined, we obtain $\frac{|cxe^{i\phi_+} + be^{i\phi_b}|^2}{|xe^{i\phi_-} + 1|^2} = r$. Then $(r - c^2)x^2 + 2[r \cos(\phi_- - \phi_b) - cb \cos(\phi_+ - \phi_b)]x + (r - b^2) = 0$; therefore, the minimum of $|x|$ is $\sqrt{\frac{r - b^2}{r - c^2}}$. The parameter b^2 is expected to be less than 0.05 [11]. The parameter c , the relative magnitude of the amplitude for the WE diagram in $D^0 \rightarrow a_0(980)^+ \pi^-$ over that in $D^0 \rightarrow a_0(980)^- \pi^+$, can be estimated from the largest re-scattering contribution, which is $\frac{B(D^0 \rightarrow K^+ K^{*-})}{B(D^0 \rightarrow K^- K^{*+})}$ [34], therefore $c^2 \sim 0.3$. It follows that we can expect that $b^2 < c^2$, and so $|x| > 1$.
[33] H. Y. Cheng and C. W. Chiang,

arXiv:2401.06316 [hep-ph].

- [34] In analogy to theoretical interpretations for WA process, re-scattering through $\rho\eta \rightarrow a_0(980)\pi$ and $K^*K \rightarrow a_0(980)\pi$ triangle diagrams can also be invoked to explain the large FSI in the WE process. However, since the BFs of $D^0 \rightarrow \rho^0\eta$, $D^0 \rightarrow K^{*0}\bar{K}^0$ and $D^0 \rightarrow \bar{K}^{*0}K^0$ [18] are small, the large FSI contribution is then expected

from the re-scattering of $K^{*\pm}K^\mp \rightarrow a_0(980)^\mp\pi^\pm$. While through the triangle diagram, only the re-scatterings of $K^-K^{*+} \rightarrow \pi^+a_0(980)^-$ and $K^+K^{*-} \rightarrow \pi^-a_0(980)^+$ are allowed. Therefore if the WE contribution is dominant, $r_{+/-} \sim \frac{\mathcal{B}(D^0 \rightarrow K^+K^{*-})}{\mathcal{B}(D^0 \rightarrow K^-K^{*+})}$, which is only about 0.3.